Multiwavelength Diode-Cladding-Pumped Nd^{3+}-Doped Germano-Aluminosilicate Fiber Laser

Stuart D. Jackson and Yahua Li, *Student Member, IEEE*

***Abstract*—Simultaneous multiwavelength oscillation at 1060 and 1090 nm has been produced from a free-running Nd^{3+}-doped multicomponent silica fiber laser. As a result of co-doping with both Al_2O_3 and GeO_2, the Nd^{3+} ions are situated at separate sites relating to either Al^{3+}-rich or Ge^{4+}-rich regions of the germano-aluminosilicate glass. The slope efficiency of the combined $\sim$1-μm output was $\sim$52% (56%) with respect to the launched (absorbed) pump power. The 1060-nm emission reaches threshold first because of the greater number of Nd^{3+} ions that are located at Al^{3+}-rich sites. On chopping the pump light the relaxation oscillations relating to the 1090-nm emission are antiphase with the oscillations observed with the 1060-nm emission. A degree of spectral overlap exists between the fluorescence emitted from Nd^{3+} ions located at each site. Power equalization (to $\sim$1 W each) of the 1060- and 1090-nm emissions was carried out by way of Raman amplification that occurred either internally or externally to the Nd^{3+}-doped silica fiber laser.**

***Index Terms*—Laser measurements, lasers, neodymium:solid lasers, optical fiber lasers, optical modulation.**

I. Introduction

MULTIWAVELENGTH laser oscillation of Nd^{3+}-based lasers can be made to take place from the $^4F_{3/2}$ level to various lower laser levels [1], [2] to provide output at $\sim$0.9 μm, $\sim$1 μm, and $\sim$1.3 μm or between the $^4F_{3/2}$ and $^4I_{11/2}$ levels only for multiwavelength output at $\sim$1-μm [3], [4]. Deliberately altering the losses specific to each transition in the former case or using the change in the reabsorption loss within the $^4I_{11/2}$ level in the latter case allows these transitions to oscillate simultaneously. Recently [5], simultaneous oscillation at 1050.2 and 1054.9 nm has been reported for an Nd^{3+}-doped fluoride glass laser, purportedly a result of laser oscillation from two different Nd^{3+} site subsets. The multiwavelength output from these lasers can be further modified to produce efficiently generated output at shorter wavelengths [6].

The beneficial effects of the increased solubility of the rare earth ion, the increased fluorescence intensity and the reduced levels of clustering of the rare earth ions associated with Al_2O_3 or P_2O_5 co-doping of silica are widely known [7]. Al_2O_3 or P_2O_5 co-doping of silica also presents, with respect to the $^4F_{3/2} \rightarrow {}^4I_{11/2}$ transition of Nd^{3+}, a peak fluorescence wavelength of $\sim$1060 nm [8] which provides oscillation or amplification at a similar wavelength [9]–[12]. The co-dopant Al_2O_3 in particular provides a wider site distribution for the Nd^{3+} ions leading to a reasonable degree of inhomogeneous broadening [13]. Likewise, it is also well recognized that the addition of small amounts of GeO_2 to the silica glass of the fiber core raises the refractive index, which is a necessary requirement for guiding of the light. Nd^{3+}-doped silica fibers that are co-doped with GeO_2 produce laser oscillation at a wavelength of 1088 nm [14], which is close to the peak fluorescence wavelength relating to Nd^{3+}-doped pure silica [8].

We report in this investigation the observation of simultaneous multiwavelength output (at 1060 and 1090 nm) from an Nd^{3+}-doped multicomponent silica fiber laser. By incorporating significant amounts of both Al_2O_3 and GeO_2 into the silica glass core during fabrication, the Nd^{3+} dopant ions are subsequently situated at sites relating to either Al^{3+}-rich regions or Ge^{4+}-rich regions of the germano-aluminosilicate glass. This condition allows near independent laser oscillation on the $^4F_{3/2} \rightarrow {}^4I_{11/2}$ transition at the two separate Nd^{3+} sites. Whilst a similar observation of simultaneous multiwavelength oscillation at 1064 and 1077 nm was made some time ago for an Nd^{3+}-doped GeO_2–P_2O_5 silica fiber laser [9], in this study, we examine in detail the characteristics of the multiwavelength output from the Nd^{3+}-doped germano-aluminosilicate fiber laser and in addition, the laser dynamics when the light from the pump laser is modulated. We also examine the effects from Raman amplification of the 1060- and 1090-nm emissions.

II. Experiment

The Nd^{3+}-doped fiber used for the experiments was made from the standard modified chemical vapor deposition (MCVD) and solution doping techniques. The Nd^{3+} concentration in the core of the fiber was measured to be $\sim$6000 ppm, the Al^{3+}:Nd^{3+} concentration ratio of 10:1 [13], and the GeO_2 concentration $\sim$5 mol.%. The soot was deposited at a temperature of 1550^0 C prior to solution doping and the tube sintered and collapsed at the standard temperatures. The core diameter (of 5.56 μm) and numerical aperture (NA) of 0.14 were such so as to allow for single-mode oscillation down to $\sim$1017 nm. The pump cladding had a diameter of 250 μm, a flat section milled to create chaotic pump trajectories within the pump cladding,

Manuscript received January 9, 2003; revised May 21, 2003. The work of Y. Li was supported by the International Postgraduate Research Scholarship (IPRS), funded by the Commonwealth Department of Education, Science and Training (DEST). This work was supported from the Australian Research Council and the Australian Photonics Co-operative Research Centre.

The authors are with the Optical Fiber Technology Centre, Australian Photonics CRC, The University of Sydney, Australian Technology Park, 1430 Eveleigh, Sydney, Australia

Digital Object Identifier 10.1109/JQE.2003.816094

and was surrounded by a low index UV-curable fluoro-polymer to create a large NA of 0.35 for the pump light. The effective absorption coefficient of the fiber was 0.074 m^{-1}. A fiber length of 35 m was used for the majority of the experiments, and hence, 92% of the launched pump power was absorbed in the fiber. The Nd^{3+}-doped fiber was pumped with a high power diode laser system (Fisba Optik AG, St. Gallen, Switzerland) operating at a wavelength of 805 nm. An $f = 30$ mm multilens system (Fisba Optik) was used to focus the pump light into the cladding of the fiber and provide a launch efficiency of ~47%. A broadband dichroic mirror at the input end to the fiber and Fresnel reflection at the output end to the fiber formed the fiber laser resonator.

The optical spectrum of the output was measured with either an Anritsu MS9710C or Ando AQ 6315A spectrum analyzer. The power in each individual contribution (P_{1060} and P_{1090}) was measured after the output from the fiber laser was collimated and dispersed with the use of three uncoated borosilicate prisms. This spectral separation technique was coarse enough to allow the independent measurement over the full bandwidth of each contribution whilst fine enough to spatially separate the two ~1-μm emissions. The temporal dynamics of the fiber laser output at the two ~ 1 μm wavelengths were measured simultaneously with two BPX65 Si photodiodes when the output was split and sent through two manually controlled monochromators (Bentham M300 and Bentham DM150). The output power was measured with an Ophir Orion power meter or a Melles Griot 13PEM001 power meter and the temporal characteristics recorded with an HP 54542A, 500-MHz oscilloscope after the pump light was modulated with a standard optical chopper.

III. Results

The slope efficiency of the 1060 nm, 1090 nm, and combined ~1-μm laser output was measured to be 39%, 12%, and 52% respectively with respect to the launched pump power (see Fig. 1). With respect to the absorbed pump power, the corresponding slope efficiencies are 42%, 13% and 56%. The total slope efficiency is significantly lower than the Stokes efficiency limit of ~75%. However, the level of concentration quenching resulting from cross relaxation ($^4F_{3/2}$, $^4I_{11/2} \rightarrow ^4 I_{15/2}$, $^4I_{15/2}$) which is enhanced by clustering appears to be low in this fiber. The 1060-nm emission had a threshold of ~40-mW launched pump power and the 1090-nm emission had a threshold of 180 mW. It is understood that the 1060-nm emission reaches threshold first because of the difference between the number of Nd^{3+} ions situated at Al^{3+}-rich sites compared to the number situated at Ge^{4+}-rich sites. As Al^{3+} is the only network-modifying ion added to the core of the fiber, the Nd^{3+} ions are more likely to be situated at the Al^{3+}-rich sites. These particular Nd^{3+} ions absorb a larger proportion of the pump light and hence reach threshold first. One interesting feature is the power ratio of the ~1-μm outputs, P_{1060}/P_{1090}, as a function of launched pump power (see inset of Fig. 1). We observe that the P_{1060}/P_{1090} ratio is a decreasing function of the launched pump power and decreases to value ~3.5 for large values of the launched pump power. The cause for the highly nonlinear trend in the ratio when $P_{\text{th},1090} < P_{\text{launch}} < 2$ W (where

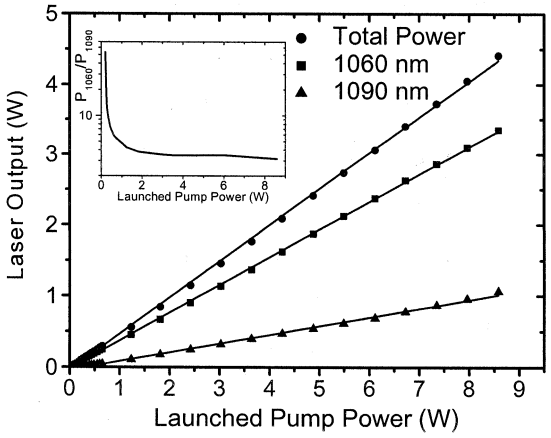

Fig. 1. Measured output power of the 1060-nm emission, 1090-nm emission, and combined emissions from the diode-pumped Nd^{3+}-doped multicomponent double-clad fiber laser as a function launched pump power into the fiber. The fiber length was 35 m. The inset displays the power ratio P_{1060}/P_{1090} of the two outputs also as a function of the launched pump power.

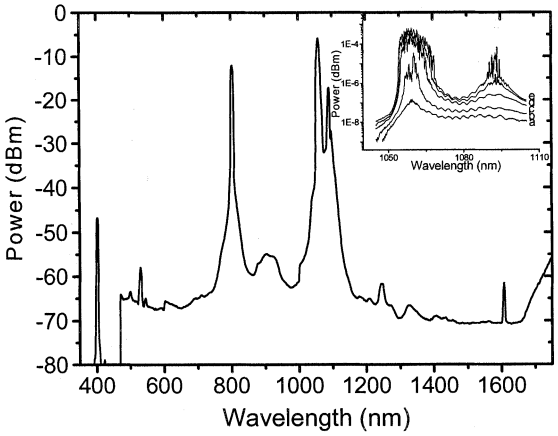

Fig. 2. Measured optical spectrum (in range 350–1750 nm) of the output from the diode-pumped Nd^{3+}-doped silica double-clad fiber laser for a pump power which has $r_{1060} = 137$. The inset displays the evolution of the dual ~1-μm outputs for **a**: $r_{1060} = 1$, **b**: $r_{1060} = 1.2$, **c**: $r_{1060} = 2.5$, **d**: $r_{1060} = 4.9$, **e**: $r_{1060} = 6.2$.

$P_{\text{th},1090}$ and P_{launch} are the launched pump power at threshold for the 1090-nm emission and the launched pump power, respectively) can be easily explained by the fact that the nonlinear region represents the transition region between the limiting cases $P_{1060}/P_{1090} = \infty$ (when $P_{\text{launch}} < P_{\text{th},1090}$) and $P_{1060}/P_{1090} \sim 3.5$ (when $P_{\text{launch}} \gg P_{\text{th},1090}$). The gradual decrease in the P_{1060}/P_{1090} ratio for $P_{\text{launch}} >\sim 6$ W relates to amplification of the 1090-nm emission at the expense of the 1060-nm emission as a result of stimulated Raman scattering (SRS) within the fiber.

Fig. 2 displays the optical spectrum in the range 350–1750 nm as measured at the fiber laser output for $r_{1060} = 137$ (where $r_{1060} = P_{\text{launched}}/P_{th,1060}$). There are a number of spectral features in addition to the pump and the two ~1-μm wavelengths. First, there exists violet emission at wavelength of 401 nm that was visible with the naked eye and was characterized by a full-width at half-maximum (FWHM) of < 1 nm. Violet emission at 412 and 381 nm has been shown to emit from Nd^{3+}-doped fluoride fiber lasers [15]. These violet emissions

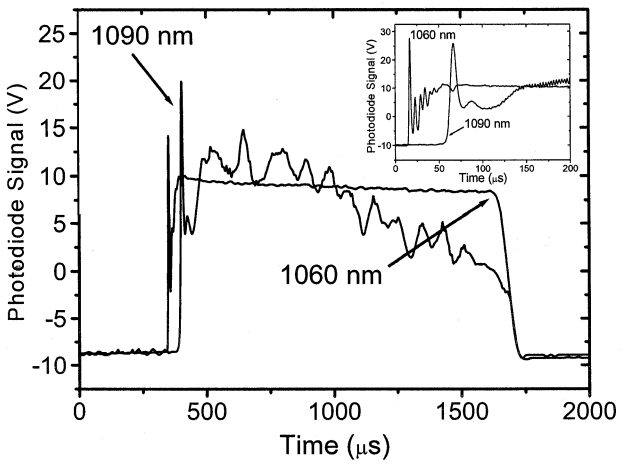

Fig. 3. Simultaneously measured 1060- and 1090-nm output from the diode-pumped Nd^{3+}-doped silica double-clad fiber laser when the 805-nm pump light was modulated at a frequency of 380 Hz and $r_{1060} = 60$. The 1090-nm signal has been enlarged in order to highlight the comparison. The inset shows in more detail the initial parts of the 1060- and 1090-nm emissions.

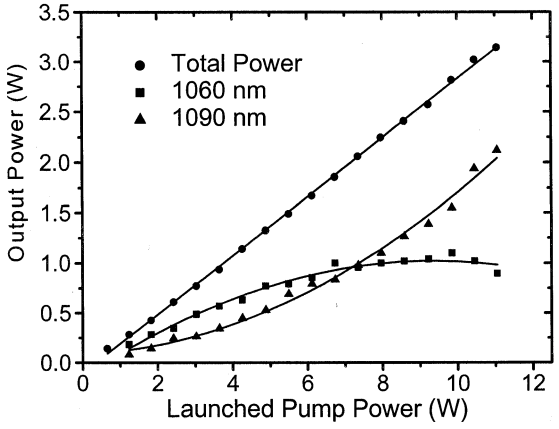

Fig. 4. Measured output power at 1060- and 1090-nm exiting 500 m of single-mode silica fiber as a function of the launched pump power into the diode-pumped Nd^{3+}-doped silica double-clad fiber laser.

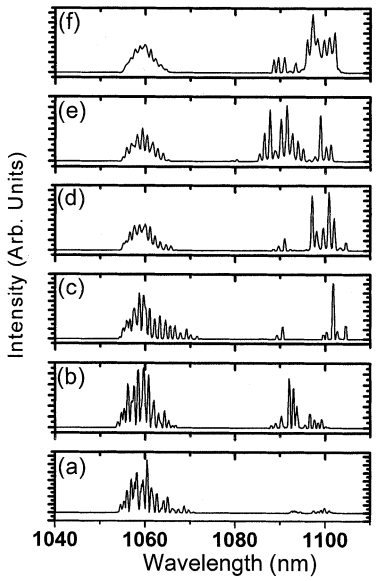

Fig. 5. Measured optical spectrum of the dual wavelength output exiting from the 500 m of single-mode silica fiber when the launched pump power into the Nd^{3+}-doped silica double-clad fiber laser was (a) 0.65 W ($r_{1060} = 16$), (b) 1.23 W ($r_{1060} = 31$), (c) 2.42 W ($r_{1060} = 61$), (d) 4.26 W ($r_{1060} = 107$), (e) 5.49 W ($r_{1060} = 137$), and (f) 6.73 W ($r_{1060} = 168$).

arise from the fluorescence transitions $^2P_{3/2} \rightarrow ^4 I_{11/2}$ and $^4D_{3/2} \rightarrow ^4 I_{11/2}$ for the 412- and 381-nm wavelengths, respectively. Fluorescence at ~381 nm was not observed in our silica-based fiber because the $^4D_{3/2}$ level is thoroughly depopulated as result of multiphonon emission to the $^2P_{3/2}$ level. A possible mechanism for populating the $^2P_{3/2}$ level is pump excited-state absorption from the $^4F_{3/2}$ level. The broad ~900-nm peak is associated with the $^4F_{3/2} \rightarrow ^4 I_{9/2}$ transition and the peak at ~1250 nm may relate to the fluorescence transition $^4F_{3/2} \rightarrow ^4 I_{13/2}$. The other peaks observed in the spectrum relate to stray light within the spectrum analyzer. The inset to Fig. 2 displays the evolution of the 1060- and 1090-nm laser output as function of r_{1060}.

Fig. 3 displays the temporal characteristic of the 1060- and 1090-nm emissions when the 805-nm pump light is modulated at a frequency of 380 Hz and the level of launched pump power adjusted so that $r_{1060} \approx 60$. As expected, the 1060-nm emission reaches threshold first ~50 μs prior to the onset of the 1090-nm emission and displays characteristic relaxation oscillations which quickly lead to continuous wave (CW) oscillation. The 1090-nm emission displays a lower level of temporal stability as compared to the 1060-nm emission: a feature that may relate to the lower pump rate for the 1090-nm emission ($r_{1090} \approx 13$). The power of the 1060-nm emission decreases slightly when the 1090-nm emission reaches threshold (see inset of Fig. 3). The wider $^4F_{3/2} \rightarrow ^4 I_{11/2}$ fluorescence associated with Nd^{3+} ions situated in Al^{3+}-rich sites overlaps with the fluorescence relating to Nd^{3+} ions situated in Ge^{4+}-rich sites and consequently, when the 1090-nm emission reaches threshold, some of the population inversion relating to Nd^{3+} ions at Al^{3+}-rich sites is depleted. This depletion is incomplete owing to the degree of site inhomogeneity.

With the use of a suitable length of single-mode silica fiber, the total power can be shared equally between the two ~1-μm emissions with the use of SRS. Fig. 4 displays the 1060 nm, the 1090 nm, and combined outputs after the dual-wavelength output from the Nd^{3+}-doped silica fiber laser is launched into 500 m of single-mode silica fiber. As the launched pump power to the Nd^{3+}-doped silica fiber laser in increased, the output at 1060 nm decreases relative to the 1090-nm output because the 1060 nm is acting as the pump for the first Stokes shift at 1090 nm. At a launched pump power into the Nd^{3+}-doped silica fiber laser of 7.2 W, the output power at 1060 and 1090 nm are near identical having a measured power of ~1 W each. (This equates to an optical-to-optical efficiency of ~77% with respect to the incident dual ~1-μm input.) On further increasing the launched pump power, the relative proportion of the total power comprising the 1090-nm emission is increased. Fig. 5 displays the spectral output as a function of launched pump power to the Nd^{3+}-doped silica fiber laser after the dual wavelength output is launched into the single-mode silica fiber. Note that the original 1090-nm output is now widened and covers the range of 1090–1100 nm.

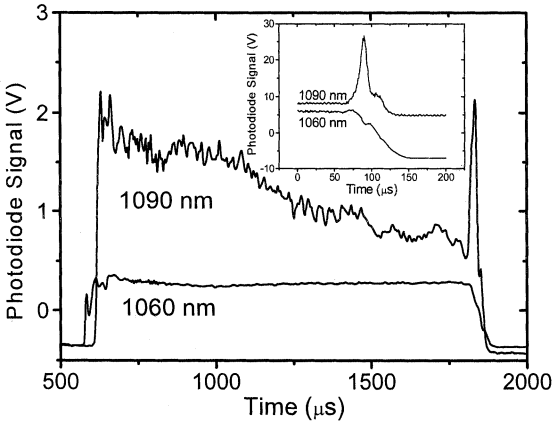

Fig. 6. Simultaneously measured 1060- and 1090-nm modulated output emitted from the 500 m of single-mode silica fiber when $r_{1060} = 137$ ($P_{launch} = 5.5$ W) and the frequency of the chopper was set at 400 Hz. The inset shows in more detail, the region toward the end of the dual wavelength emission.

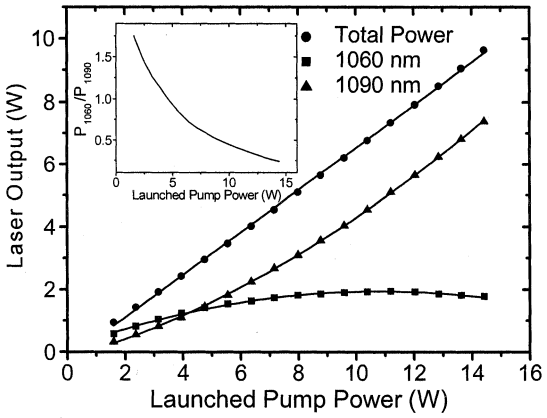

Fig. 7. Measured output power of the 1060-nm emission, 1090-nm emission, and combined emissions from a diode-pumped Nd^{3+}-doped silica double-clad fiber laser as a function launched pump power for a fiber that had a smaller effective absorption coefficient. The fiber length was 100 m. The inset displays the power ratio P_{1060}/P_{1090} of the two outputs also as a function of the launched pump power.

Fig. 6 displays the dual wavelength emission that exits the single-mode silica fiber when the pump power to the Nd^{3+}-doped silica fiber laser is chopped. We can observe the normal relaxation oscillations relating to each emission present at the beginning of the pulse. Toward the end of the 1090-nm emission, however, we observe a sharp spike in the 1090-nm emission with a corresponding dip in the 1060-nm emission (see inset of Fig. 6). The origin of this spike in the 1090-nm emission after passing through the single-mode fiber is currently under investigation. However, the dip in the 1060-nm emission relates to cross saturation between the pump (1060 nm) and Stokes (1090 nm) waves [16].

IV. Discussion

The results presented above indicate that two practically isolated laser systems are operating in this fiber laser. Nd^{3+}-doped aluminosilicate fiber lasers and Nd^{3+}-doped germanosilicate fiber lasers in separate configurations and under free-running conditions lase at 1060 and 1088 nm, respectively. In the fabrication of our fiber, reasonably large quantities of Al_2O_3 and GeO_2 were used for dissolution of Nd^{3+} clusters and for raising the core refractive index. The fact that the fiber laser oscillates at wavelengths close to those related to the isolated fiber laser systems indicates that most of the Nd^{3+} ions are situated in regions dominated by either aluminosilicate or by germanosilicate glass. Phase separation of the binary silicate glasses themselves strongly relates to the ionic potential ($= Z/r$, where Z is the valence and r is the ionic radius) of the network modifying cations [17], whereby the greater the ionic potential, the greater the region of immiscibility. In general, the aluminosilicate glasses are very miscible, whereby the Al^{3+} ions are generally Si-substitutional in which three Si-substitutional Al^{3+} ions in close proximity have the charge compensated by a fourth Al^{3+} ion accommodated in the interstitial part of the silica network [18]. For the Al_2O_3 and GeO_2 concentration levels used here, both the binary silicate glasses should display no independent phase separation. Since Ge^{4+} is a network former and Al^{3+} a network modifier, the Nd^{3+} ions are perhaps doped into a fully miscible glass system that has Ge^{4+}-rich regions and Al^{3+}-rich regions. (Spectral hole burning in conjunction with a single Nd^{3+} site and full miscibility of the two binary silicate glasses could be operating, however, the fact that the thresholds for each emission are close does not support this hypothesis.) Factors such as the soot deposition temperature, which influences the porosity of the glass, and the different ion exchange rates of the Nd^{3+} and Al^{3+} ions during the doping phase of the fiber fabrication process will also influence the distribution of dopant ions. Clearly, more work is required to fully characterize this multicomponent glass system.

The use of SRS to equate the power levels of 1090- and 1060-nm laser emissions has been shown to be simple and efficient and hence of interest to a number of applications. At higher values of the launched pump (1060 nm) power; practically all of the 1060-nm emission could be converted to the 1090-nm emission. With the incorporation of Bragg gratings for the Nd^{3+}-doped germano-aluminosilicate fiber laser, the spectrally complex output shown in Fig. 5 could be further refined.

Fig. 7 displays the 1060- and 1090-nm output from a Nd^{3+}-doped germano-aluminosilicate fiber laser which utilizes a fiber that has an effective absorption coefficient of 0.032 m^{-1} a core diameter of 4.39 μm and NA of 0.17 and thus supported single mode operation down to ~975 nm. The Al^{3+}:Nd^{3+} concentration ratio was 15:1 and the Nd^{3+} concentration similar to the previous fiber. The pump diameter of this fiber was 300 μm and hence enabled a higher launch efficiency of 60%. 100 m of this fiber was used for the experiments and 96% of the launched pump power was absorbed. The measured slope efficiency of 65% with respect to the launched pump power for this fiber laser can be accounted for by the fact that the higher Al^{3+}:Nd^{3+} concentration ratio should lead to lower $^4F_{3/2}$ level lifetime quenching and the increase in the fractional amount of launched pump light that is absorbed. The 1090-nm emission was the dominant output when $P_{launch} > 4.5$ W. The change in the P_{1060}/P_{1090} ratio with the launched pump power also displays very different behavior as compared to the previous fiber. This behavior can be explained by the fact

that the factor-of-three increase in the length of fiber required for efficiently generated output increases the level of SRS in the Nd^{3+}-doped germano-aluminosilicate glass fiber laser and hence we observe a strong transference from the 1060-nm emission to the 1090-nm emission. With careful control and monitoring of the fiber fabrication parameters, the fiber composition can be tailored according to the desired output required from the fiber laser.

The use of multicomponent glasses for the creation of multiwavelength output with the same dopant ion allows a number of possibilities. The wide 30-nm separation between the emission wavelengths of this device will provide for applications such as differential absorption spectroscopy. Combining the three main co-dopants of silica namely, GeO_2, Al_2O_3, and P_2O_5 together in various ratios could allow for laser oscillation on a number of wavelengths using a single rare earth ion transition in which the ion is situated in a number of quite different sites.

V. Conclusion

We have demonstrated the simultaneous oscillation at 1060 and 1090 nm from a diode-cladding-pumped Nd^{3+}-doped multicomponent silica glass fiber laser. The slope efficiency of the 1060- and 1090-nm emission was measured to be 39% and 12%, respectively, with respect to the launched pump power and 42% and 13% with respect to the absorbed pump power. For values of the launched pump power well above the threshold level, the power ratio of the 1060-nm output to the 1090-nm output was approximately 3.5:1 when $L = 35\ m$. On modulating the 805-nm pump light, there existed anti-phase dynamics between the 1060- and the 1090-nm emissions as a result of the spectral overlap between the fluorescence arising from Nd^{3+} ions situated in Al^{3+}-rich sites and from Nd^{3+} ions situated in Ge^{4+}-rich sites. On passing the dual-wavelength $\sim$1-μm output from the Nd^{3+}-doped silica fiber laser through 500 m of single-mode silica fiber, we observed that at a launched pump (805 nm) power of 7.2 W, the power was shared equally (to $\sim$1W) between the 1-μm emissions because of transference from the 1060-nm emission to the 1090-nm emission as a result of SRS.

Acknowledgment

The authors appreciate discussions with S. Fleming and the fiber fabrication skills of T. Ryan.

References

[1] C. G. Bethea, "Megawatt power at 1.318 μ in Nd^{3+}:YAG and simultaneous oscillation at both 1.06 and 1.318 μ," *IEEE J. Quantum Electron.*, vol. QE-9, pp. 254–254, Feb. 1973.

[2] M. Nakazawa and Y. Kimura, "Simultaneous oscillation at 0.91, 1.08 and 1.53 μm in a fusion-spliced fiber laser," *Appl. Phys. Lett.*, vol. 51, no. 22, pp. 1768–70, 1987.

[3] K. Otsuka, "Simultaneous oscillations of different transitions in lasers," *IEEE J. Quantum Electron.*, vol. QE-14, pp. 1007–13, Dec. 1978.

[4] K. Otsuka, R. Kawai, Y. Asakawa, P. Mandel, and E. A. Viktorov, "Simultaneous single-frequency oscillations on different transitions in a laser-diode-pumped $LiNdP_4O_{12}$ laser," *Opt. Lett.*, vol. 23, no. 3, pp. 201–3, 1988.

[5] J. Azkargorta, I. Iparraguirre, R. Balda, J. Fernandez, J. L. Adam, E. Denoue, and J. Lucas, "Site-effects on the laser emission of Nd^{3+} ions in a new fluoride glass," *J. Non-Cryst. Solids*, vol. 213–214, pp. 271–5, 1997.

[6] K. Otsuka, R. Kawai, and Y. Asakawa, "Intracavity second-harmonic and sum-frequency generation with a laser-diode-pumped multitransition-oscillation $LiNdP_4O_{12}$," *Opt. Lett.*, vol. 24, no. 22, pp. 1611–13, 1999.

[7] K. Arai, H. Namikawa, K. Kumata, T. Honda, Y. Ishii, and T. Handa, "Aluminum or phosphorus co-doping effects on the fluorescence and structural properties of neodymium-doped silica glass," *J. Appl. Phys.*, vol. 59, no. 10, pp. 3430–6, 1986.

[8] J. Stone and C. A. Burrus, "Neodymium-doped silica lasers in end-pumped fiber geometry," *Appl. Phys. Lett.*, vol. 23, no. 7, pp. 388–9, 1973.

[9] I. D. Miller, D. B. Mortimore, P. Urquhart, B. J. Ainslie, S. P. Craig, C. A. Millar, and D. B. Payne, "A Nd^{3+}-doped CW fiber laser using all-fiber reflectors," *Appl. Opt.*, vol. 26, no. 11, pp. 2197–201.

[10] K. Liu, M. Digonnet, H. J. Shaw, B. J. Ainslie, and S. P. Craig, "10 mW superfluorescent single-mode fiber source at 1060 nm," *Electron. Lett.*, vol. 23, no. 24, pp. 1320–1, 1987.

[11] T. Miyazaki, Y. Karasawa, and M. Yoshida, "Neodymium-doped fiber amplifier at 1.064 μm," *Electron. Lett.*, vol. 30, no. 25, pp. 2142–3, 1994.

[12] H. Zellmer, U. Willamowski, A. Tunnermann, H. Welling, S. Unger, V. Reichel, H.-R. Muller, T. Kirchhof, and P. Albers, "High-power cw neodymium-doped fiber laser operating at 9.2 W with high beam quality," *Opt. Lett.*, vol. 20, no. 6, pp. 578–80, 1995.

[13] S. Sen, "Atomic environment of high-field strength Nd and Al cations as dopants and major components in silicate glasses: A Nd L_{III}-edge and Al K-edge X-ray absorption spectroscopic study," *J. Non-Cryst. Solids*, vol. 261, no. 1-3, pp. 226–36, 2000.

[14] R. J. Mears, L. Reekie, S. B. Poole, and D. N. Payne, "Neodymium-doped silica single-mode fiber lasers," *Electron. Lett.*, vol. 21, no. 17, pp. 738–40, 1985.

[15] D. S. Funk, J. W. Carlson, and J. G. Eden, "Room-temperature fluorozirconate glass fiber laser in the violet (412 nm)," *Opt. Lett.*, vol. 20, pp. 1474–1476, 1995.

[16] S. D. Jackson and P. H. Muir, "Theory and numerical simulation of nth-order cascaded raman fiber lasers," *J. Opt. Soc. Amer. B*, vol. 18, no. 9, pp. 1297–306, 2001.

[17] P. Hudon and D. R. Bake, "The nature of phase separation in binary oxide melts and glasses. I. silicate systems," *J. Non-Cryst. Solids*, vol. 303, no. 3, pp. 299–345, 2002.

[18] J. Laegsgaard, "Theory of Al_2O_3 incorporation in SiO_2," *Phys. Rev. B*, vol. 65, no. 17, pp. 174 104/1–16, 2002.

Stuart D. Jackson received the B.Sc. degree in 1989 and the B.Sc. (Hons.) degree in 1990, both from the University of Newcastle, Newcastle, Australia, and the Ph.D. degree from the Centre for Lasers and Applications, Macquarie University, Sydney, Australia, in 1996.

In 1995, he joined the Laser Photonics Group at the University of Manchester, Manchester, U.K., and carried out post-doctoral research into high-power fiber lasers. In 1999, he joined the Optical Fiber Technology Centre at the University of Sydney, Sydney, Australia, where he is now an Australian Research Fellow sponsored directly by the Australian Research Council. His interests include diode-pumped solid-state lasers, spectroscopy and philosophy.

Yahua Li (S'03) was born in Yueyang, China, in 1966. He received the B.E and M.M. degrees from Huazhong University of Science and Technology (HUST), Wuhan, China, in 1988 and 2001, respectively. He is currently working toward the Ph.D. degree in the Optical Fiber Technology Centre, University of Sydney, Sydney, Australia, in the area of high-power fiber lasers.

During 1988–2002, he was with the National Research Center for Laser Technology and Engineering, HUST. In 1998, he was promoted to Associate Professor. He also worked at Huagong Laser Company, Wuhan, China, where he was a Section Manager, responsible for research and development, manufacturing, quality control, and marketing. His research interests include development of high-power solid-state Nd:YAG lasers for biomedical and commercial applications.